

Original article

Movable oil content evaluation in low-to-medium maturity lacustrine shale during *in-situ* conversion

Guoshuai Bai^{1,2}, Guohui Chen¹*, Zhongxian Cai²*, Hongxing Yan³, Shuangfang Lu¹, Ahmed E. Radwan⁴

¹Sanya Offshore Oil & Gas Research Institute of Northeast Petroleum University, Sanya 572025, P. R. China

²School of Earth Resources, China University of Geosciences (Wuhan), Wuhan 430074, P. R. China

³Research Institute of Oil Exploration and Development, Liaohe Oilfield of Petrochina, Panjin 124010, P. R. China

⁴Institute of Geological Sciences, Jagiellonian University, Kraków 30-387, Poland

Keywords:

In-situ conversion
numerical simulation
movable oil
hydrocarbon generation
Damintun Sag

Cited as:

Bai, G., Chen, G., Cai, Z., Yan, H., Lu, S., Radwan, A. E. Movable oil content evaluation in low-to-medium maturity lacustrine shale during *in-situ* conversion. *Advances in Geo-Energy Research*, 2025, 16(1): 77-90.

<https://doi.org/10.46690/ager.2025.04.08>

Abstract:

Low-to-medium maturity shale oil resources hold significant potential, but their economic accessibility is limited by low porosity, low permeability, and a low proportion of movable oil. *In-situ* conversion technology can crack organic matter and in-place oil into lighter molecules, enhancing oil and gas mobility and improving recovery rates. The success of this approach depends on dynamically evaluating the amount of movable shale oil during *in-situ* conversion. This study targets the lower submember of the fourth member of the Eocene Shahejie Formation (Lower Sha4 Member) in the Damintun Sag, Bohai Bay Basin, China. Through thermal simulation experiments, organic geochemical experiments, and nuclear magnetic resonance experiments, shale residual oil evaluation, organic matter hydrocarbon generation process evaluation, and dynamic evaluation of immovable oil were carried out. By integrating numerical simulations of the temperature field with the experimental results, a dynamic evaluation method for movable resources in shale during *in-situ* conversion was established. The findings indicate that the conversion rates of kerogen-to-oil and kerogen-to-gas first increase and then gradually stabilize as thermal maturity increases, with oil generation reaching its peak when the vitrinite reflectance reaches 1.0%. Long-term preserved shale samples were identified to contain immovable oil, the content of which increases with maturity before peaking and then declining. *In-situ* conversion of low-to-medium maturity shale in the upper part of the model can significantly increase movable oil resources in a year, potentially reaching the levels of extractable medium-to-high maturity shale. This work presented a crucial approach for assessing and improving *in-situ* conversion technology, providing a means of maximizing economic feasibility.

1. Introduction

Shale oil, a significant unconventional resource, is classified based on maturity (Vitrinite Reflectance, R_o) into low-to-medium ($R_o = 0.5\%-1.0\%$) and medium-to-high ($R_o > 1.0\%$) categories (Zhao et al., 2018). The exploitation of medium-to-high maturity shale oil, characterized by lighter hydrocarbon components and higher movable oil content, can

be achieved through the implementation of horizontal well hydraulic fracturing technology. Conversely, low-to-medium maturity shale oil exhibits higher viscosity and lower movable oil content, requiring the application of retorting technology to enable the conversion of solid kerogen into liquid products for effective development (Feng et al., 2020; Jin, 2023). The *in-situ* conversion process is a retorting method that entails

the pyrolysis of kerogen in shale to achieve the generation of oil and gas products, which demonstrates considerable potential in promoting the recovery of shale oil resources (Jin et al., 2023). This technology can be categorized into four distinct classifications according to the method of heating: combustion heating, conduction heating, convection heating, and radiation heating (Sun et al., 2023). Among these, the *in-situ* heating conduction technology has proven to be the most mature and has achieved significant success in the field tests (Zhao et al., 2018).

The *in-situ* conversion of shale involves multiple thermo-physical and thermochemical processes, including the generation of hydrocarbons from organic matter, the transformation of inorganic minerals, the evolution of pore structure, and the consequent alterations in shale oil's retention capacity (Li et al., 2024a; Dong et al., 2025). Previous studies have investigated the evolution of porosity, permeability, pore structure, and hydrocarbon generation of organic matter during the artificial thermal maturation of shale, as well as the hydrocarbon generation amount during *in-situ* conversion (Zhang et al., 2019; Wei and Sheng, 2022; Zhang et al., 2022; Wu, 2023). However, existing research predominantly focuses on the laboratory scale but fails to be further extended to the geological scale, with limited attention to the changes in the mobility of low-to-medium maturity shale oil during *in-situ* conversion. Understanding the increase and evolution of movable oil content is essential for optimizing *in-situ* conversion development and the maximization of benefits. In this paper, movable oil content refers to the total amount of liquid hydrocarbons generated by shale, excluding the immovable oil that remains in the shale. Therefore, the dynamic evaluation of the movable shale oil content during *in-situ* conversion involves the following key aspects: (1) dynamic evaluation of the temperature evolution in shale reservoirs; (2) dynamic evaluation of the hydrocarbon generation in shale; (3) dynamic evaluation of changes in movable oil content in conjunction with the evolution of bound oil capacity (Wei and Sheng, 2022).

The dynamic evaluation of temperature evolution in shale reservoir during *in-situ* conversion requires numerical simulations (Li et al., 2024b; Wang et al., 2024a). These simulations not only address complex problems that theoretical research cannot solve, but also provide crucial support for formulating *in-situ* conversion extraction schemes. By now, extensive research has been conducted on numerical simulations of the *in-situ* heating and oil shale cracking process. Kang et al. (2020) conducted a comprehensive analysis of temperature field evolution during *in-situ* electric heating of oil shale, utilizing heat conduction models and three-dimensional finite element analysis. Lei et al. (2024) investigated the effects of different well patterns (triangular, square, and hexagonal) on *in-situ* heating efficiency of oil shale, finding the hexagonal arrangements are the most efficient and economical. By comparing numerical simulation results for different heating methods, Shi et al. (2014) found that horizontal wells in thin-layer oil shale formations reduce heat loss by approximately 10% compared to vertical wells. Recently, Wu (2023) further explored the impacts of varying heating power settings,

heating temperature, well spacing, and heating patterns on the economic benefits of *in-situ* heating of low-maturity oil shale based on numerical simulation of the temperature field. However, it is noteworthy that most existing research has focused on low-maturity oil shale, with relatively insufficient research on low-to-medium maturity shale. Despite this, their collective efforts have laid a solid foundation for temperature field simulation of low-to-medium maturity shale during *in-situ* conversion.

For the dynamic evaluation of hydrocarbon generation from shale during *in-situ* conversion, it is essential to have a comprehension of how organic matter generates hydrocarbons under geological conditions. This process can be evaluated using experimental simulations, basin modeling, and hydrocarbon generation kinetics (Hunt, 1979; Tissot and Welte, 1984; Liao et al., 2018). Among these methods, hydrocarbon generation kinetic has been widely used to evaluate the hydrocarbon generation in organic matter under geological conditions due to its ability to derive specific kinetic parameters based on the characteristics of the source rock (Braun and Burnham, 1992; Burnham, 2017). The key to this method is selecting a suitable reaction kinetic model and obtaining accurate kinetic parameters. At present, the parallel first-order reaction model is extensively utilized due to its ability to accurately simulate the hydrocarbon generation process of organic matter that closely matches actual geological conditions (Behar et al., 2008). The key kinetic parameters can be obtained through rapid temperature rise simulations in the laboratory based on the time-temperature compensation relationship (Zhang et al., 2022). Based on the above research, some scholars have exploratively extended hydrocarbon generation kinetics from geological conditions to the *in-situ* conversion process of shale oil (Zhang et al., 2019, 2022). Their findings support the application of hydrocarbon generation kinetics in *in-situ* conversion studies and underscore the importance of dynamic evaluations of hydrocarbon generation for these processes. However, a key distinction exists between hydrocarbon generation evaluations under *in-situ* conversion and geological conditions. The former begins with the source rocks at a low maturity stage with the residue oil bearing in the pores, while the latter starts from the immature stage with no residue oil. Therefore, both the secondary cracking of retained oil and newly generated oil must be considered in dynamic evaluations during *in-situ* conversion.

Only the oil that can flow in shale has the potential to be exploited, so the evaluation of movable oil content is crucial to identify the "sweet spots" (Jarvie, 2012a; Larter et al., 2012; Tian et al., 2024). Various methods have been utilized to assess oil mobility, each with specific strengths and limitations. Among these, multistep rock-eval pyrolysis method has gained widespread acceptance as a technique for characterizing oil mobility by simulating hydrocarbon release under progressive thermal cracking (Hu et al., 2021). Nuclear Magnetic Resonance (NMR), when paired with centrifugation or displacement techniques, offers a comprehensive analysis of fluid mobility across varying pore sizes. The Oil Saturation Index (OSI) method sets varying lower limits for movable oil based on the region or geological layer, highlighting its

regional specificity (Pepper and Corvi, 1995; Jarvie, 2012a). The multi-step solvent extraction method (Hu et al., 2021) quantifies oil content but has limitations in differentiating adsorbed oil from free oil during shale heating or extraction. The adsorption-free oil model method enhances these approaches by distinguishing between adsorbed and free oil. However, it also acknowledges that not all free oil within shale's micro-nano pore structures is movable, thus providing only an estimate of potential movable oil content (Li et al., 2019a). Despite these advances, current methodologies predominantly focus on medium-to-high maturity shale, with limited assessments of movable oil during the *in-situ* conversion of low-to-medium maturity shale. Therefore, there is an imperative for the development of a methodology that can effectively evaluate the movable oil content of *in-situ* conversion in low-to-medium maturity shale.

To address the above scientific issues, this paper selects low-to-medium maturity shale samples from the Lower Sha4 Member of the Bohai Bay Basin for relevant experiments and research. The Lower Sha4 Member shale exhibits exceptional geochemical characteristics for *in-situ* conversion, with total organic carbon (TOC) values up to 16.99 wt.% and R_o predominantly within 0.5%-1.0% (Chen et al., 2017). These parameters align with the widely accepted favorable conditions for *in-situ* conversion, namely a TOC content over 6% and an R_o value between 0.5% and 1.0% (Zhao et al., 2018). This study investigates low-to-medium maturity shale from the Lower Sha4 Member through integrated thermal simulation, organic geochemical analysis, and NMR experiments to characterize residual oil content, hydrocarbon generation processes, and immovable oil distribution. A dynamic assessment methodology for movable oil resources during *in-situ* conversion has been developed by coupling temperature field modeling with the Easy% R_o model.

2. Samples and methods

2.1 Samples

The shale samples utilized in this study were exclusively obtained from the Lower Sha4 Member in the Damintun Sag, specifically from Wells S352 and A17. The Damintun Sag is situated in the northeastern of the Liaohe Depression within the Bohai Bay Basin, China (Fig. 1) (Chen et al., 2017; Chen et al., 2020). The principal oil-bearing shale in the Damintun Sag occurs in the Paleogene Shahejie Formation, which is comprised of four distinct members: Sha4, Sha3, Sha2, and Sha1 Members, from bottom to top (Li et al., 2019b). With the subsidence of the Bohai Bay Basin and the rise in the lake level, the depositional environment of the Sha4 Member transitioned from a semi-deep lake to a deep lake, resulting in the deposition of multiple black shale layers (Chen et al., 2020).

2.2 Experiments and methods

2.2.1 Thermal simulation experiments

Sample A17-1 from Well A17 at a depth of 2,472.26 m was selected for open system hydrocarbon generation kinetics

simulation (Table S1). The simulation was performed using a Rock-Eval 6 rock pyrolyzer. The procedure involved: (1) crushing the shale sample to approximately 80 mesh, and weighing 10-60 mg of the sample on the sample boat; (2) heating the analyzer to 200 °C and holding for 3 min to remove free hydrocarbons; (3) heating the sample to 600 °C at 10 °C/min and 20 °C/min, while recording product quantities in real-time; (4) collecting pyrolysis products at 30 °C intervals within the same temperature range and heating rates for gas chromatography analysis (PY-GC) to quantify gas (C_1 - C_5) and liquid (C_{5+}) components. Sample A17-2 was divided into seven blocks, six of which (A17-3-A17-8) were heated from 200 °C to different temperatures (364.1, 400.5, 426.5, 443.2, 473.8 and 526.3 °C) at a rate of 20 °C/h. The corresponding vitrinite reflectance values (Easy% R_o) were calculated for these temperatures as 0.7%, 0.9%, 1.1%, 1.3%, 1.7%, and 2.5%, respectively, using the Easy% R_o method (Sweeney and Burnham, 1990). These experiments were conducted at the Guangzhou Institute of Geochemistry without applying water or pressure.

2.2.2 Rock pyrolysis, TOC, R_o and chloroform extraction

The samples, both naturally matured and thermally simulated, underwent a surface cleaning and pulverization process to 80-100 mesh. TOC contents were subsequently measured with a Leco CS-230 carbon and sulfur analyzer, following the removal of carbonates with 5% hydrochloric acid at 80 °C. For pyrolysis analysis, the Rock-Eval 6 instrument detected free hydrocarbons (S_1) at 300 °C and cracking hydrocarbons (S_2) from 300 to 650 °C, also recording the peak temperature (T_{max}) of S_2 . Furthermore, the samples underwent Soxhlet extraction using chloroform at 70 °C for over 72 hours to analyze the oil content. Subsequent pyrolysis of these extracted samples yielded data on S_1 , S_2 and T_{max} after extraction (S_1' , S_2' and T_{max}'). The naturally matured shales were selected for the purpose of measuring the R_o using a UMSP50 microphotometer.

2.2.3 NMR experiments

The NMR experiments were conducted using a MicroMR23-060H-1 instrument, which operates at a frequency of 21.36 MHz, with a magnet strength of 0.50 T and a magnetic temperature of 32 °C. The NMR testing parameters included a Wait Time (TW) of 1,000 ms, a Receiver Gain 1 (RG1) of 20 dB, a Digital Receiver Gain 1 (DRG1) of 3, a Pulse Repetition Gradient (PRG) of 3, a Spectral Width (SW) of 333.33 kHz, a Time Domain (TD) of 421,224, a Number of Echoes (NECH) of 6,000, an Echo Time (TE) of 0.21 ms, a first pulse length (P_1) of 5.40 μ s, a second pulse length (P_2) of 10.60 μ s, and a Number of Scans (NS) of 64.

2.2.4 Numerical simulation of temperature field

The temperature field simulation was conducted using COMSOL Multiphysics, a finite element analysis software developed by COMSOL Inc., in Stockholm, Sweden (Jin et al., 2023). To simulate the *in-situ* heating conversion process of shale, this study established a porous medium heat conduction model. The basic assumptions of the model, the energy conservation equation, and the initial and boundary conditions

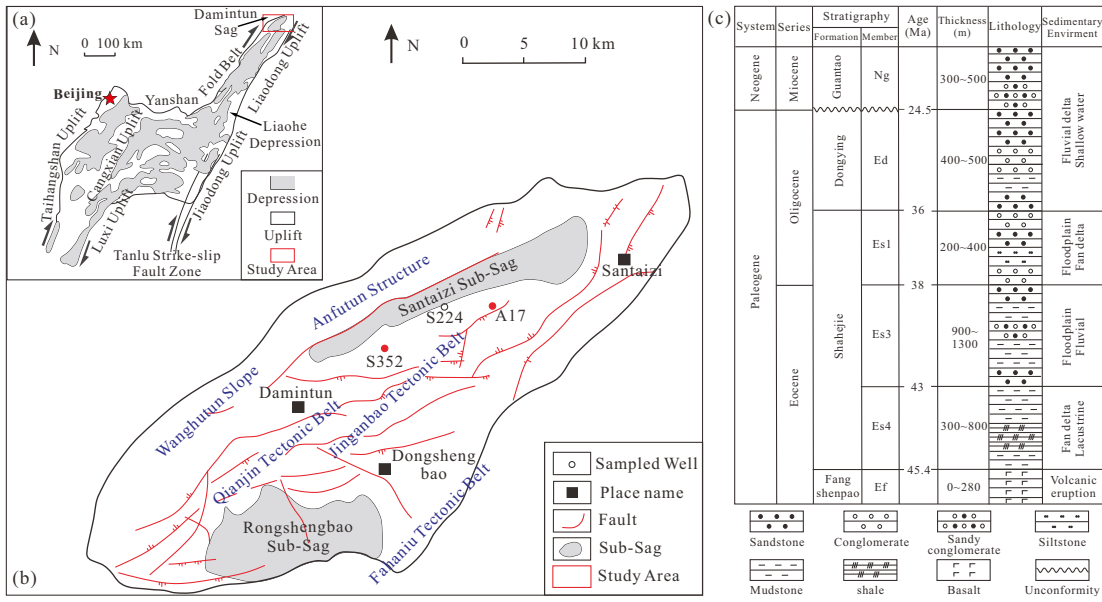


Fig. 1. Location and stratigraphic column of the Damintun Sag, Bohai Bay Basin. (a) Location of the Damintun Sag; (b) tectonic units of the Damintun Sag with the specific positions of Wells A17 and S352 and (c) the Cenozoic stratigraphy and sedimentary characteristics of the Damintun Sag (modified from Chen et al. (2018) and Chen et al. (2020)).

of the temperature field are consistent with our previous study (Bai et al., 2024).

A three-dimensional geometric model, measuring $1,200 \times 150 \times 240 \text{ m}^3$, was established based on *in-situ* conduction conversion technology, as illustrated in Fig. 2. The model was created to represent the lithological composition of the strata in the depth range of 3,130-3,370 m in the Lower Sha4 Member of Well S352, featuring layers of mudstone, shale, and sandstone. This model adopted a regular hexagonal well pattern with a side length of 15 m and employed a horizontal well heating method. The heating wells were maintained at a constant temperature of $600 \text{ }^\circ\text{C}$, with a length set to 1,000 m. After establishing the three-dimensional geometric model, it was imported into COMSOL for grid partitioning. To ensure the precision of the temperature field simulation results, an extremely fine grid division form was used, resulting in 951,492 grid elements. The details of the input parameters are provided in Table S2.

2.2.5 Evaluation method of resource quantity

Given the exploration degree and geological conditions of the area under study, this research employs the volume method from the statistical category to predict resource intensity. The specific calculation followed Eq. (14) from Li et al. (2016). The organic logging response model involved in the formula, which calculates the continuous vertical distribution of geochemical parameters, follows the Back Propagation (BP) neural network method (Senthil et al., 2012). The resource evaluation began by converting an unstructured grid, obtained from the initial grid division, into a structured grid to facilitate subsequent resource calculation. The temperature data from all points within the unstructured grid region were imported into a custom Python program. A structured grid model was then reconstructed, where each grid point was represented as a

cube with an edge length of 0.1 m. The KDTree algorithm was employed to efficiently locate the coordinates of different grid points, with corresponding temperatures determined through cubic spline interpolation.

After obtaining the hydrocarbon conversion rates and the results of the regular grid division, the three-dimensional datasets for kerogen to oil, kerogen to gas, and oil to gas rates were calculated through interpolation. Since the *in-situ* heating model is based on the Lower Sha4 Member of Well S352, these datasets can be combined with the comprehensive geochemical profile of this interval to calculate the hydrocarbon generation at each grid point in the model. The specific calculation formulas are as follows:

$$q_o = SH\rho S_2^0(X_o - X_o^0) \quad (1)$$

$$q_g = SH\rho S_2^0(X_g - X_g^0) \quad (2)$$

$$q_{og} = q_o X_{og} \quad (3)$$

$$q_{ro} = SH\rho S_1^0(1 - X_{og}) \quad (4)$$

$$q_{rog} = SH\rho S_1^0 X_{og} \quad (5)$$

$$q_{to} = q_o + q_{ro} - q_{og} \quad (6)$$

$$q_{tg} = q_g + q_{og} - q_{rog} \quad (7)$$

where X_o^0 and X_g^0 are the kerogen to oil conversion rate and the kerogen to gas conversion rate at the initial state ($t = 0$), respectively. X_o , X_g and X_{og} are the conversion rate of kerogen to oil, kerogen to gas and oil to gas, respectively. S_1^0 and S_2^0 are the original free hydrocarbon content and the

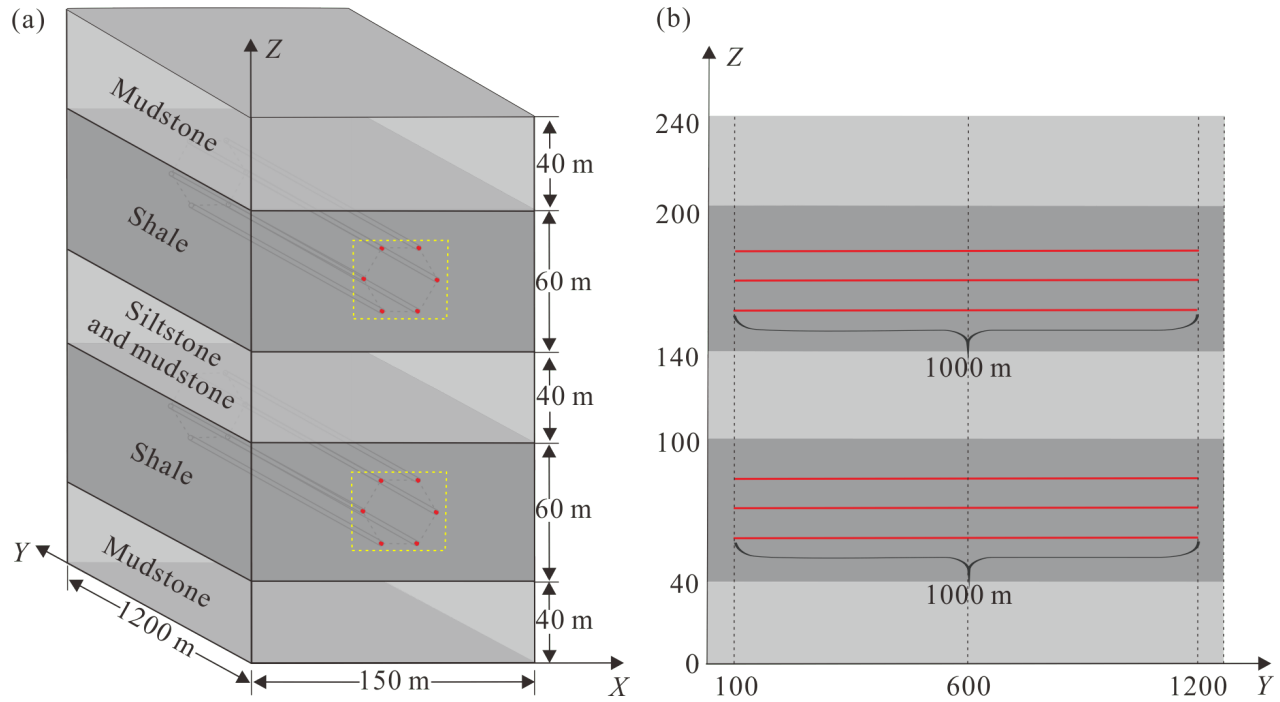


Fig. 2. Geometric model and heating scheme for *in-situ* heating in the Lower Sha4 Member. (a) The three-dimensional diagram of the model and (b) the YZ profile of the model.

original pyrolysis potential, respectively, mg/g. q_o , q_g , q_{og} , q_{ro} and q_{rog} are the amounts of oil generation by kerogen, gas generation by kerogen, gas generation from the oil produced by kerogen, residual oil and gas generated from residual oil at each grid within the heating model, respectively, t; q_{to} is the total oil content at each grid point, t; q_{tg} is the total gas content at each grid point, t; S is the bottom area of each model grid, m^2 ; H is the height of each model grid, m; ρ is the rock density, which is 2.65 t/m^3 (Li et al., 2016).

To avoid including unheated areas in the resource evaluation results, only areas with hydrocarbon conversion rates greater than 10% are considered effective heating areas. The cumulative oil and gas resources within all grids in the effective heating range of the shale represent the oil and gas resources in the heating model. The Z coordinate of each grid center corresponds to the actual depth. The final step involves calculating the movable amount of shale during the *in-situ* heating, based on the three-dimensional dataset of R_o and the relationship between immovable oil content per unit TOC and R_o :

$$Q_{mo} = \sum_{i=1}^n (q_{toi} - q_{bi}) \quad (8)$$

$$Q_m = \sum_{i=1}^n (q_{tgi} + q_{toi} - q_{bi}) \quad (9)$$

where Q_{mo} and Q_m are the movable oil amount and the movable hydrocarbon amount, respectively, t; q_b is the immovable oil content per unit TOC at each grid point, t; i represents the i -th grid point, ranging from 1 to n ; n is the total number of grid points.

3. Results

3.1 Hydrocarbon generation thermal simulation experiment

The efficiency curves for hydrocarbon production of the sample at varying heating rates can be acquired through the hydrocarbon generation kinetics simulation. As the heating rate increases, the conversion rate curve shifts rightward toward higher temperatures, indicating that higher temperatures are required to achieve the same conversion rates at faster heating rates (Fig. 3(a)). This shift reflects the compensatory relationship between time and temperature in the thermal evolution of organic matter, which is constrained by the reaction time available for kerogen hydrocarbon generation.

This study employs a finite parallel first-order kinetic model, featuring a consistent frequency factor but varying activation energies, to derive the hydrocarbon generation kinetic parameters of shale samples (Arrhenius, 1889). Detailed methodologies for calibrating the dynamic parameters can be found in the literature (Lu et al., 1996). By fitting the data using hydrocarbon generation kinetics software, the activation energy and pre-exponential factor (A) of the sample were determined. The activation energy distribution for the kerogen-to-oil conversion is relatively broad, ranging from 160 to 340 kJ/mol (Fig. 3(b)). Calculated frequency factors for kerogen-to-oil and kerogen-to-gas conversions are 2.78×10^{11} and $2.49 \times 10^{11} \text{ s}^{-1}$, respectively. Previous studies have shown that the organic matter type of the shale in the Lower Sha4 Member is mainly type I (Chen et al., 2017). Therefore, the oil-to-gas kinetic model of Pepper and Corvi (1995),

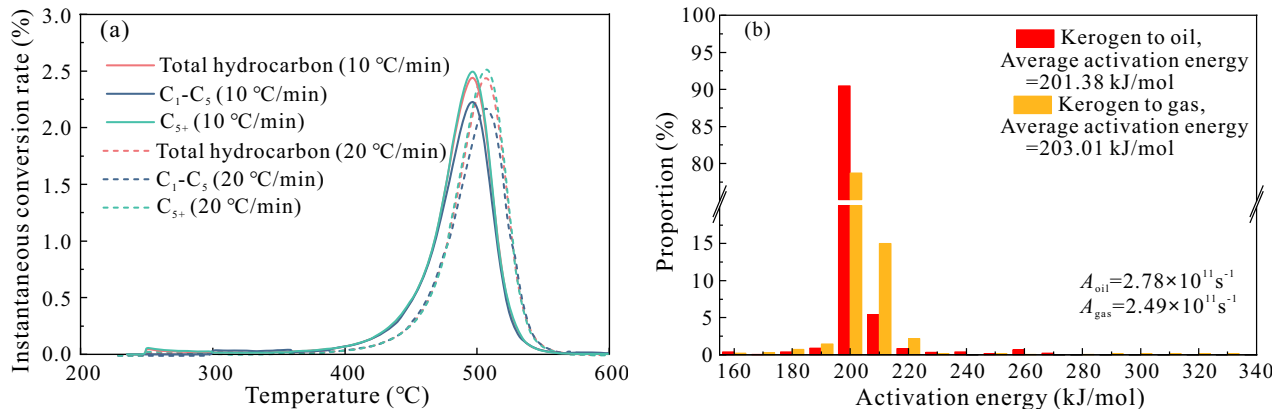


Fig. 3. (a) The relationship between instantaneous conversion rates and heating temperatures at two different heating rates and (b) distribution of activation energy for kerogen-to-oil and kerogen-to-gas conversions.

which is applicable to type I organic matter, was chosen to simulate the kinetic parameters of oil-to-gas conversion in the study area. The activation energy distribution for oil-to-gas conversion is narrower, ranging from 210.9 to 277.9 kJ/mol, with a primary peak at 244.4 kJ/mol and a frequency factor of $9.99 \times 10^{13} \text{ s}^{-1}$. Overall, the average activation energy for kerogen-to-oil, kerogen-to-gas, and oil-to-gas conversions increases sequentially, suggesting that kerogen-to-oil conversion occurs more readily than the other transformations. The concentrated activation energy distribution in the source rocks of the Lower Sha4 Member, characterized by a prominent peak, indicates a potential for rapid hydrocarbon generation once the corresponding temperatures are reached.

3.2 Comparison of pyrolysis results before and after extraction

The geochemical parameters of naturally matured and thermal simulation shale samples from Wells S352 and A17 are shown in Table S3. Naturally matured shales from Well S352 have an average R_o of 0.85% (ranging from 0.65% to 0.98%), an average TOC of 4.98% (ranging from 0.47% to 9.46%), and an average free hydrocarbon content (S_1) of 2.04 mg/g (ranging from 0.22 to 5.72 mg/g). After chloroform extraction, the TOC, referred to as TOC', drops to an average of 4.37% (ranging from 0.33% to 8.29%), and the extracted free hydrocarbon content (S_1') drops to an average of 0.09 mg/g (ranging from 0.03 to 0.18 mg/g). In contrast, the shale samples of different maturities from Well A17 have a notably higher TOC (ranging from 7.28% to 12.99%), higher S_1 (ranging from 0.52 to 3.04 mg/g), higher TOC' (ranging from 6.98% to 12.25%), and higher S_1' (ranging from 0.12 to 0.38 mg/g). After extraction, the T_{max} either increase or decrease compared to those before extraction. However, overall, most shale samples exhibit an increase in T_{max} following extraction. These observations suggest that the organic matter in the Lower Sha4 Member is relatively abundant, and the maturity predominantly falls within the low to medium range. Additionally, the shale exhibits favorable oil-bearing properties.

3.3 NMR experiment

Based on previous classifications (Mehana and Elmonier, 2016; Li et al., 2018; Li et al., 2020; Wang et al., 2024b), the T_1 - T_2 map of shale samples in the study area is divided into five regions: (1) kerogen/solid organic matter ($T_2 < 0.2 \text{ ms}$, $T_1 > 10 \text{ ms}$), (2) adsorbed/heavy hydrocarbons ($0.2 \text{ ms} < T_2 < 1 \text{ ms}$, $T_1/T_2 > 10 \text{ ms}$), (3) free/light hydrocarbons ($T_2 > 1 \text{ ms}$, $T_1/T_2 > 10 \text{ ms}$), (4) hydroxyl/structured water ($T_2 < 0.2 \text{ ms}$, $T_1 < 10 \text{ ms}$), and (5) pore water ($T_2 > 0.2 \text{ ms}$, $T_1/T_2 < 10 \text{ ms}$) (Fig. 4). Using these criteria, NMR signals from various regions in the T_1 - T_2 correlation spectra of shales in different states are identified. As shown in Table S4, NMR signal amplitudes per unit mass in naturally matured samples show considerable variation. For total organic matter, the range is 18.46 to 271.65 a.u., with an average of 135.55 a.u. Kerogen exhibits amplitudes from 0 to 145.12 a.u. (average 65 a.u.), bound oil from 0 to 102.87 a.u. (average 37.42 a.u.), and free oil from 0 to 80.66 a.u. (average 33.13 a.u.). In thermally simulated samples, the signal amplitudes for total organic matter and total oil per unit mass initially increase and then decrease as maturity progresses, highlighting the impact of hydrocarbon generation from organic matter on shale oil content.

3.4 Numerical simulation of temperature field

The yellow box areas in the upper and lower parts of the front view of the model were selected to observe the temperature field changes (Fig. 2(a)). The temperature profile in the lower part of the model is shown in Fig. S1, while the temperature profile in the upper part of the model is shown in Fig. 5. As the heating time progresses, the temperature of the shale layer experiences a continuous increase, with the average temperature within the hexagonal well pattern eventually stabilizing at approximately 300 °C. From the profile, it is observed that the temperature distribution at various times is axisymmetric along the vertical axis, with a greater extent of heat influence in the horizontal direction compared to the vertical. This phenomenon is attributed to the higher transverse thermal conductivity of shale relative to its

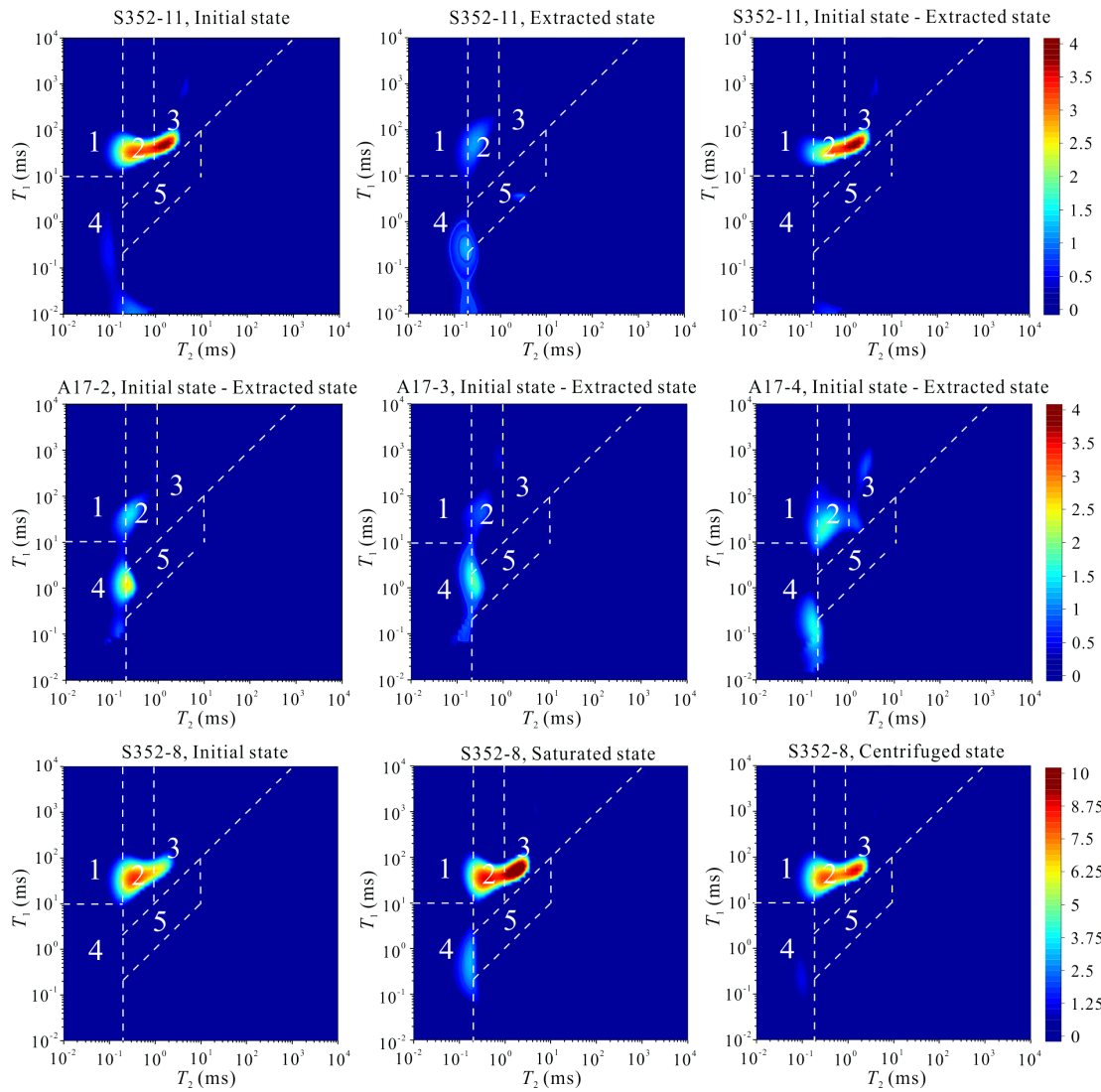


Fig. 4. NMR T_1 - T_2 map of naturally matured and thermally simulated shale samples in different states.

longitudinal thermal conductivity (Wang et al., 2019). In the first year of heating, the heated area is mainly concentrated around the heating wells. By the third year, the heated areas between the heating wells begin to overlap. By the ninth year, the six heating wells collectively transfer heat to the surrounding area. The majority of energy input occurs during the initial decade of heating, followed by a stabilization of the average temperature.

4. Discussions

4.1 Residual oil evaluation

In evaluating shale oil resources, S_1 is typically used as an indicator of the free hydrocarbon content in shale. However, relying solely on S_1 to represent residual hydrocarbons may lead to underestimation, as it may overlook heavy hydrocarbons recorded in S_2 and light hydrocarbons that volatilized during sample storage and preparation. To ensure an accurate evaluation of shale oil resources, it is crucial to correct for light hydrocarbons lost and adjust for heavy hydrocarbons within

the S_1 measurement. The recovery methods for light and heavy hydrocarbons in S_1 follows Li et al. (2016). This systematic correction and compensation for the loss of light and heavy hydrocarbons at varying depths within the shale enhance the accuracy of the hydrocarbon content estimation.

However, S_1 data from laboratory experiments alone may not suffice for a comprehensive three-dimensional characterization of the source rock's entire volume. This limitation can significantly impede the detailed quantitative assessments required for evaluating hydrocarbon generation and expulsion, as well as for calculating residual oil resources. To overcome this, it is imperative to integrate high-resolution vertical geophysical logging methods with laboratory tests. This approach ensures a more precise estimation of residual oil resources. In this study, a BP neural network method was utilized to predict TOC, S_1 , and S_2' of the Lower Sha4 Member in Well S352 of the Damintun Sag. Leveraging the results of the light and heavy hydrocarbon corrections, the neural network enabled the determination of the longitudinal distribution of the original residual oil amount (S_1^0) in Well S352 (Fig. 6).

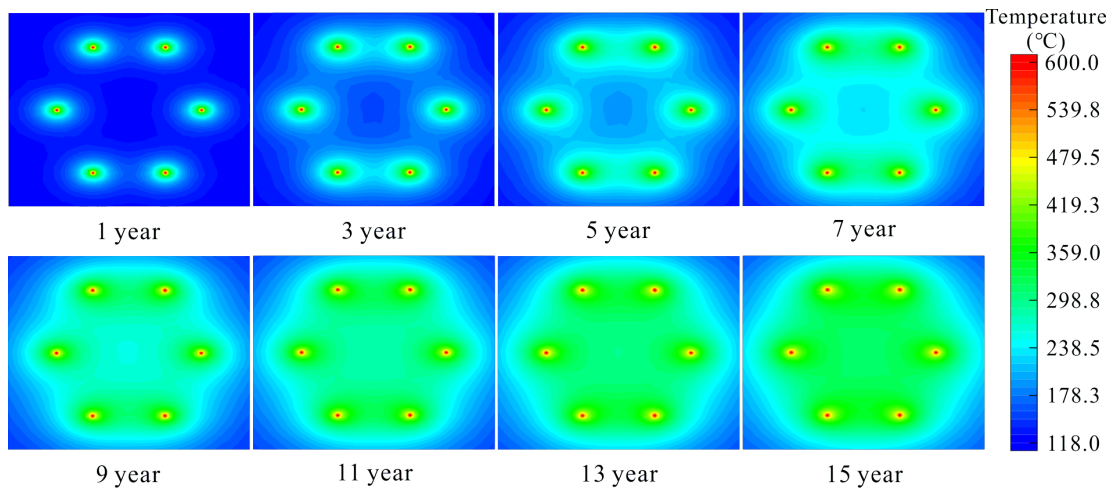


Fig. 5. Temperature distribution and its evolution within the reservoir in the upper part of the numerical model during *in-situ* conversion.

From the profile, it can be observed that the average original residual oil content of shale in the upper part of the numerical model is higher than that from the lower part, which are 11.60 and 4.27 mg/g respectively. Through this method, a detailed characterization of the vertical heterogeneity of the source rock was achieved, providing a logging calibration basis for subsequent quantitative calculations of source rock resources.

4.2 Assessment of hydrocarbon generation process

The conversion rate is commonly used to represent the hydrocarbon generation process, reflecting the extent of organic matter evolution and conversion of kerogen into oil and gas. It can be used to calculate the amount of hydrocarbon generated (Pan et al., 2018). Utilizing the kinetic parameters for kerogen-to-oil, kerogen-to-gas, and oil-to-gas conversions-calibrated from prior experimental results-and incorporating the burial and thermal history model parameters of the study area, a kinetic geological extrapolation was conducted. This extrapolation produced the profile of conversion rates for kerogen to oil, kerogen to gas, oil to gas, total oil, and total gas in the target strata of the study area (Fig. 7). The relationship between conversion rates and maturity forms the basis for calculating hydrocarbon generation during *in-situ* conversion. According to the classical hydrocarbon generation model for kerogen proposed by Tissot and Welte (1984), the thermal maturation of organic matter in the source rocks of the study area can be categorized into four distinct stages of hydrocarbon generation.

The four stages are as follows: (1) Early oil generation stage: At this stage, $\text{Easy}\%R_o$ ranges from 0.5% to 0.8%. Kerogen primarily produces oil, and the conversion rate of kerogen to oil is higher than that of kerogen to gas. (2) Condensate oil generation stage: During this stage, with $\text{Easy}\%R_o$ ranging from 0.8% to 1.5%, kerogen continues to be the dominant source of oil generation. However, early-generated oil also begins to crack into light hydrocarbons, and gas production from kerogen becomes significant. (3) Oil-to-gas

stage: In this stage, occurring from $\text{Easy}\%R_o$ 1.5% to 2.5%, the conversion of early-generated oil into gas is significant. As maturity increases, the conversion rates of kerogen to oil and gas remain constant, the net oil conversion rate continuously decreases, and the oil to gas conversion rate steadily increases. (4) Dry gas stage: When $\text{Easy}\%R_o$ exceeds 2.5%, this stage is defined by the cracking of C_{2-5} hydrocarbons into methane. Almost all liquid hydrocarbons are consumed due to secondary cracking, and the generated hydrocarbons are predominantly gaseous.

4.3 Evolution of immovable oil

Using the NMR calibration method and the relationship between NMR calibration coefficient values of fluid signals and maturity established by Li et al. (2022), the NMR signal values from T_1 - T_2 maps of shale oil with varying maturities can be converted into oil content. As shown in Table S4, the oil content in naturally matured samples ranges from 1.05 to 17.97 mg per gram of rock (averaging 7.71 mg/g rock) and from 0.42 to 3.29 mg per gram of TOC (averaging 1.85 mg/g TOC). The oil content of shale samples, calculated using the pyrolysis parameter ($S_1+\Delta S_2$), is presented in Table S3. It can be seen from the data that there is a positive correlation ($R^2=0.76$) between the oil content of naturally matured samples obtained by NMR method and the $S_1+\Delta S_2$ obtained by the pyrolysis method. Combined with the correlation coefficient obtained by Li et al. (2022), it can be seen that the NMR method can be used to predict the content of shale oil.

NMR experiments were conducted on shale samples in their initial, oil-saturated, and centrifuged states to determine whether the shale oil in the samples is movable. Taking S352-8 as an example, the free oil signal intensity of the NMR T_1 - T_2 map increases significantly in the oil-saturated state compared to the initial state (Fig. 4). This increase suggests that prolonged storage led to hydrocarbon loss, leaving the residual oil in the shale unsaturated. After centrifugation, the signal intensity in region 3 decreases, indicating that some oil is removed by this process. However, when comparing the ce-

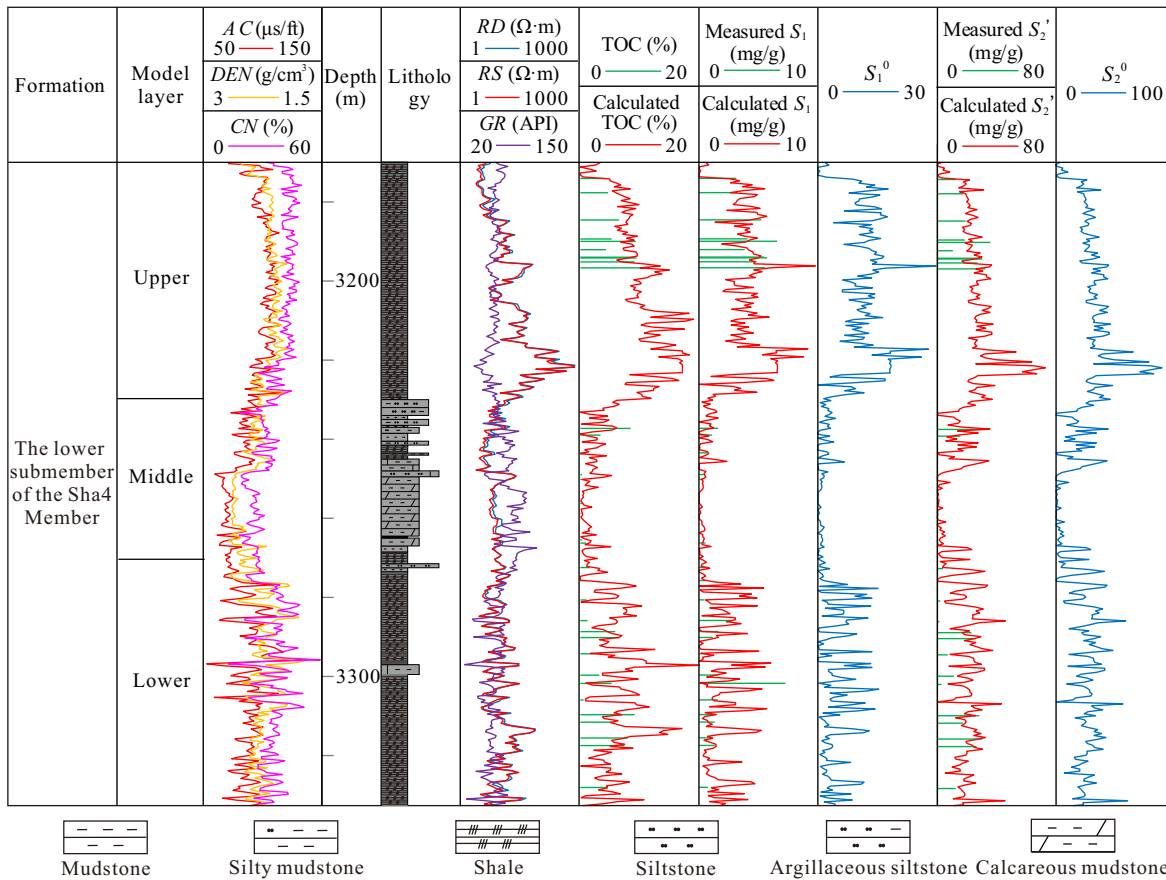


Fig. 6. Comprehensive geochemical profile in the Lower Sha4 Member of Well S352.

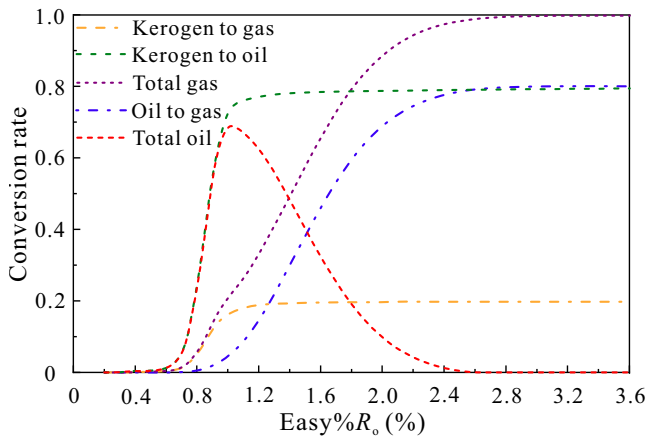


Fig. 7. The conversion rate chart of the Shahejie Formation in the Damintun Sag.

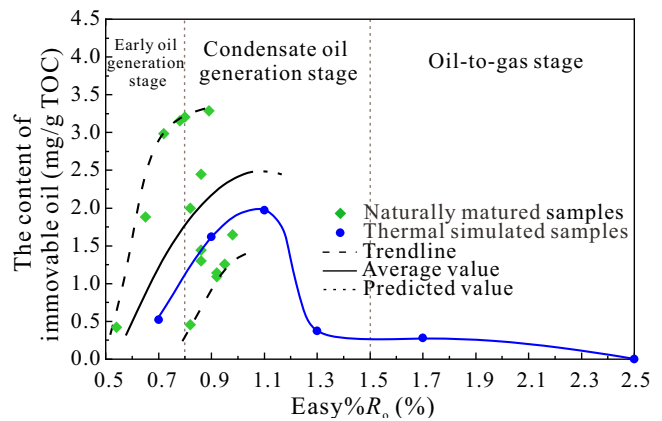


Fig. 8. Relationship between immovable oil content and maturity ($Easy\%R_o$) in naturally matured and thermal simulated samples.

ntrifuged state to the initial state, the signal intensity for shale oil remains higher in the centrifuged state. This finding supports the notion that both bound and free oil in shales—especially those stored for extended periods—are largely immovable. In addition, Jarvie (2012b) proposed an index for determining shale oil mobility, known as the OSI ($OSI = S_1/TOC \times 100$), based on production practice. When the OSI is greater than 100 mg/g, shale oil is considered to be in a movable state. However, calculations using the data in Table S3 show that the OSI for the shale samples ranges from 4.36

to 80 mg/g. This result indicates that residual oil stored in shale for extended periods is predominantly in an immobile state.

According to the above analysis, the calculated oil content is essentially equivalent to the immovable oil content. Integrating this data with the organic matter hydrocarbon generation evolution model allows establishing a relationship between immovable oil content and maturity (Fig. 8). Overall, the content of immovable oil in shale exhibits an initial rise followed by a decline as maturity increases. In the early oil

generation stage, the amount of oil generated by kerogen increases with maturity, leading to enhanced adsorption of hydrocarbons onto kerogen surfaces due to its higher porosity and polar functional groups (Xu et al., 2018). This results in increased immovable oil content within the shale. During the condensate oil generation stage, kerogen reaches its peak oil generation capacity. However, the adsorption capacity of kerogen begins to decline as thermal maturation alters its chemical structure (e.g., loss of oxygen-containing groups and aromatic condensation), reducing its ability to retain hydrocarbons (Liang et al., 2023). Concurrently, the cracking of early-generated oil into light hydrocarbons and gas generation by kerogen further contribute to the decrease in immovable oil content. In the oil-to-gas stage, as maturity exceeds 1.5%, the progressive cracking of oil into gas becomes dominant, while the adsorption capacity of kerogen diminishes significantly due to graphitization (Hou et al., 2024). By the time maturity reaches 2.5%, nearly all the early-generated oil has cracked into gas, and the immovable oil content drops to 0 mg/g TOC.

4.4 Evaluation of the movable oil content within shale during *in-situ* conversion

By applying the resource evaluation methodology for *in-situ* conversion, the movable resources within the shale model can be quantitatively assessed. For brevity, this paper focuses specifically on the shale in the upper part of the model, examining variations in maturity, oil generation conversion rate, movable oil quantity, and movable hydrocarbon quantity during *in-situ* conversion. The resulting distribution and evolution of maturity and oil generation conversion rate during *in-situ* conversion in the upper part of the model are depicted in Fig. S2. Analysis indicates that due to the rapid rate of temperature increase near the heating wells, the maturity and conversion rate of shale reach their maximum values relatively quickly. After 15 years of heating, the shale within the well pattern of six heating wells essentially reaches the overmature stage ($\text{Easy}\%R_o > 2.0\%$), suggesting that the hydrocarbon generation process is nearly complete. The conversion rate of oil generation increases with heating time, but not linearly. It rises sharply in the early stages and more gradually in the later stages. By the 11th year, the conversion rate in the hexagonal well pattern approaches 1, indicating near-complete oil generation.

The distribution and evolution of movable oil during *in-situ* conversion in the upper part of the numerical model are shown in Fig. 9(a). As heating progresses, areas around the heating wells increasingly lack movable oil, primarily due to the temperature rise causing both residual and newly generated oil in the shale to crack into lighter hydrocarbons. The deeper shale, being buried deeper and reaching the peak of kerogen to oil conversion earlier, contains higher movable oil content compared to shallower shale within the hexagonal heating well pattern. Overall, the movable oil content in shale first increases and then decreases over time, with the peak of kerogen-to-oil conversion occurring around the 11th year of heating. Fig. 9(b) shows the distribution and evolution of movable hydrocarbons during *in-situ* conversion. Due to kerogen-to-oil and oil-to-gas

conversions, the amount of movable hydrocarbons at the same location exceeds that of movable oil. As heating time extends, the quantity of movable hydrocarbons gradually increases, surpassing 1×10^{-4} t at all grid points in the hexagonal well pattern by the 15th year.

The relationship between effective resource quantity and heating time during *in-situ* conversion for shale shows that the upper part of the model exhibits a higher resource quantity compared to the lower part (Figs. 10(a) and 10(b)). This difference is attributed to the lower maturity, higher hydrocarbon generation potential, and greater abundance of organic matter in the upper part of the model. During the 15-year heating process, there is a significant increase in the amount of hydrocarbon generation, oil generation, and movable hydrocarbons in the early stages of heating, but this growth rate slows down in the later stages. This trend suggests that the hydrocarbon generation potential of shale within a specific area during *in-situ* conversion is inherently limited. Furthermore, the quantities of residual oil, movable oil, and total oil in the shale from both the upper and lower parts of the model do not increase continuously with heating; they increase and then decrease. The decline in movable oil resource quantity could be due to the cracking of oil generated during later stages of heating. Based on the grid quantity and the volume of the effective heating area in the model, resource quantities for different heating times were calculated. Combining these calculations with shale density allows for the calculation of resource quantities per unit mass of rocks at different heating times.

The correlation between heating time and total oil content, movable oil content, and movable hydrocarbon content per unit mass of rock is shown in Figs. 10(c) and 10(d). Initially, the total oil content in the shale from the upper part of the model is 12.91 mg/g, with movable oil content at 0.68 mg/g. In contrast, the total oil content in the shale from the lower part of the model starts at 4.60 mg/g, with no movable oil present initially. As heating progresses, the effective heating volume of both the upper and lower shale gradually expands. However, the total oil content and movable oil content do not increase linearly but fluctuate, with peaks in oil content noted in the tenth year of heating. Overall, the total oil content and movable oil content in the shale from the upper part of the model are consistently higher than that from the lower part of the model. The *in-situ* heating modification effect and mining potential of the shale are superior in the upper part of the model compared to the lower part, due to the higher organic matter abundance and lower maturity of the upper shale.

Based on the above analysis, it is evident that *in-situ* conversion of low-to-medium maturity shale can significantly increase the volume of movable resources. To further evaluate the effectiveness of *in-situ* heating and assess its exploitation potential, comparing it with exploitation cases of medium-to-high maturity shale-where stable industrial oil and gas flows have been achieved-provides valuable insights. For instance, the Q2 oil layer of the Qingshankou Formation in Well GY-8, located in the Gulong Sag of the Songliao Basin in China, serves as a representative case. This oil layer currently achieves a daily oil production of 16.2 tons and a daily gas

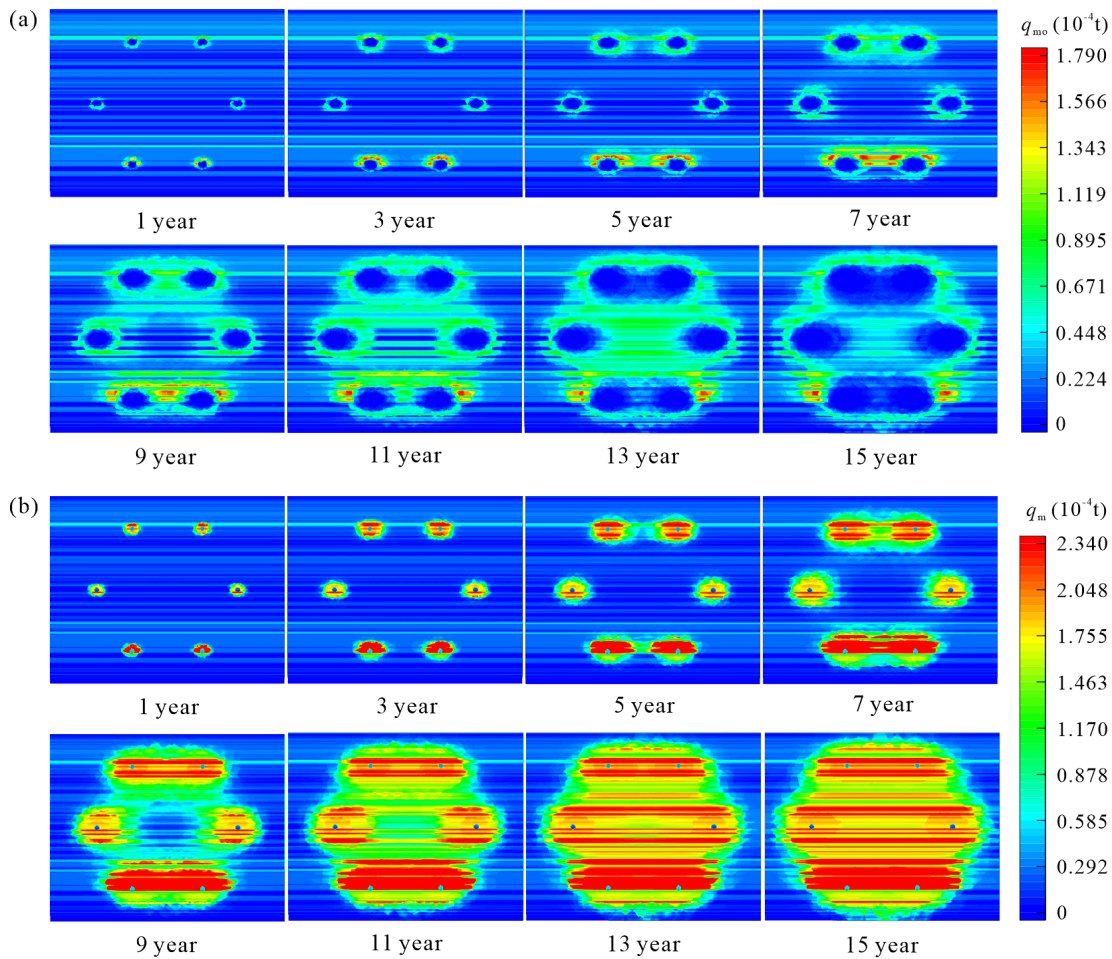


Fig. 9. Distribution and evolution of movable oil and movable hydrocarbon during *in-situ* conversion in the upper part of the numerical model. (a) movable oil and (b) movable hydrocarbon.

production of 6,459 m³. The average movable oil content per unit mass of shale in this layer is approximately 12.88 mg/g (the green marker line in Fig. 10(c)). If this value is taken as a reference, the movable oil content of the shale in the upper part of the model can reach or approach this level within the first year through *in-situ* conversion. This indicates that after reasonable technical interventions, low-to-medium maturity shale can exhibit significant development potential in a short period of time and is expected to achieve efficient and stable exploitation. It should be noted that the movable oil content of 12.88 mg/g serves merely as a reference value for the development of low-to-medium maturity shale oil resources. In practical applications, this value should be adjusted based on specific geological conditions and detailed economic analyses.

4.5 Implications for economic viability and future research directions

The economic viability of *in-situ* conversion technology hinges on achieving an energy efficiency ratio greater than 1 (Lu et al., 2023). This ratio is defined as the energy of produced hydrocarbons divided by the sum of energy consumed in shale heating and the energy-equivalent of engineering and

post-operational costs. If engineering operation costs are not considered, the energy efficiency ratio needs to be at least 3 to have the potential to reduce engineering costs through large-scale operations and achieve profitable development. Research indicates that the energy gained from the generation of oil and gas is approximately 18.9 to 29.9 times the energy consumed by organic matter cracking (energy efficiency ratio), indicating the potential to be economically efficient (Lu et al., 2023). The energy efficiency ratio, after considering the energy consumed by the inorganic components of the shale in absorbing heat and the energy consumed by the surrounding rock in dissipating heat, increases with the increase in TOC content. When the TOC content is greater than 4.2% (energy efficiency ratio of 3), it is expected that through large-scale operations, engineering costs can be diluted, making the energy efficiency ratio greater than 1 after considering engineering costs. That is, at this point, *in-situ* conversion technology can be economically viable. Given that the heating well temperature in this study is 600 °C, the well spacing is 15 m, and the average TOC value of the Lower Sha4 Member samples is 4.98%, the energy efficiency ratio can reach over 4, which strongly indicates that the heating scheme in this study is capable of achieving profitable development of low-to-medium maturity shale oil in

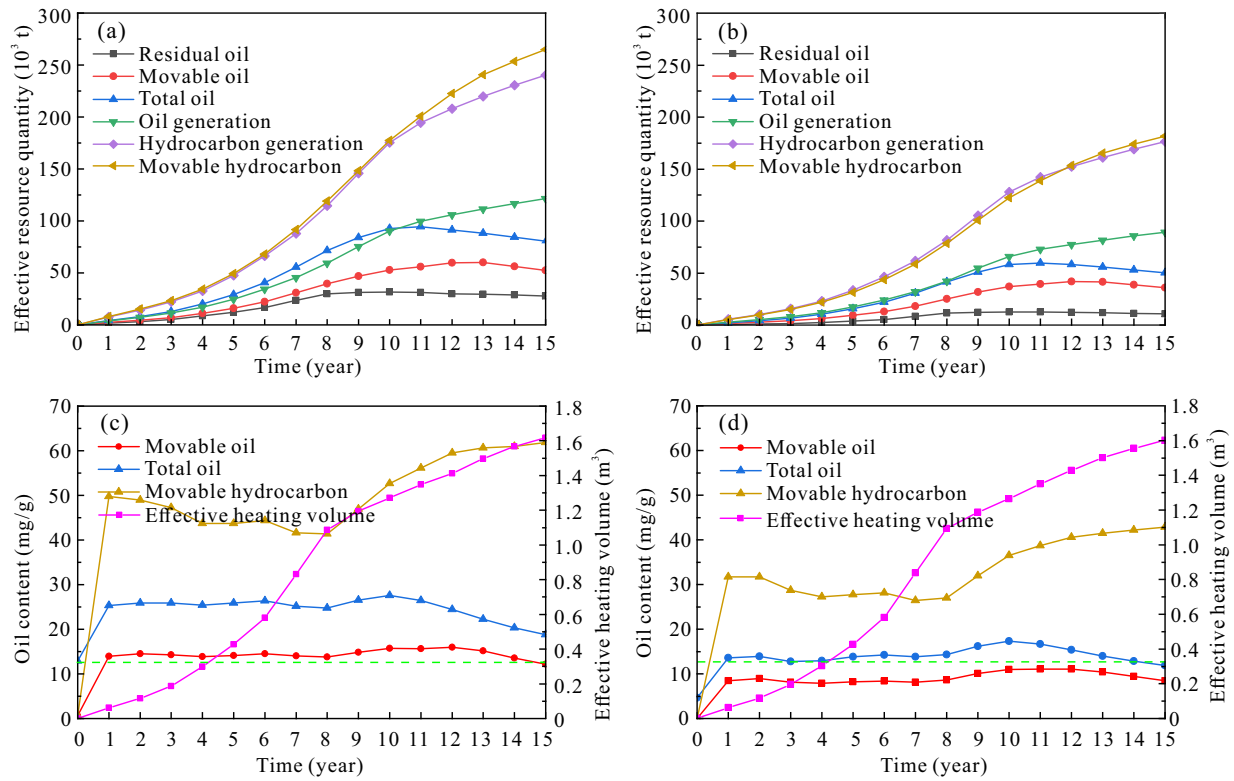


Fig. 10. The relationship between effective resource quantity, oil content, and heating time during *in-situ* conversion. (a) Effective resource quantity in the upper part of the model; (b) effective resource quantity in the lower part of the model; (c) oil content in the upper part of the model and (d) oil content in the lower part of the model.

the Lower Sha4 Member.

Future research should focus on optimizing heating parameters and improving model accuracy to enable more precise control and cost-effective development. As technologies continue to advance, the green and efficient development of shale oil is expected to make significant contributions to the diversification and sustainability of the global energy supply. A number of areas are suggested for additional investigation in order to build on the results of this study and address any outstanding issues. First, to verify the laboratory and numerical simulation results in real-world settings, pilot-scale *in-situ* conversion initiatives should be carried out. Second, more studies should look into how geological variability affects *in-situ* conversion efficiency. Examples of this variety include mineral composition, thermal maturity, and the amount of organic matter.

Third, it is important to evaluate how *in-situ* conversion affects the environment, taking into account subsurface changes, water use, and greenhouse gas emissions. Fourth, more complex geological and thermal dynamics, like multiphase fluid flow and heterogeneous reservoir characteristics, should be incorporated into sophisticated numerical models. Lastly, it should be investigated whether *in-situ* conversion can be combined with other enhanced oil recovery methods such as hydraulic fracturing or CO_2 injection. Combining these techniques could further improve resource usage and recovery rates. The entire potential of *in-situ* conversion technology

can be achieved by tackling these research areas, opening the door for the sustainable and profitable exploitation of shale oil resources with low-to-medium maturity. In addition to promoting energy security, this will help the shift to resource extraction methods that are more ecologically conscious and efficient.

5. Conclusions

The present investigation of shale samples from the Damintun Sag, Bohai Bay Basin, has resulted in the establishment of a novel methodology for the evaluation of movable resources within shale during *in-situ* conversion. The key findings are summarized as follows:

- 1) The corrected results for light and heavy hydrocarbon yields indicate that the original residual oil content of the shale from the upper part of the numerical model (average 11.6 mg/g) is higher than that from the lower part of the model (average 4.27 mg/g).
- 2) The hydrocarbon generation kinetics method demonstrates that the conversion rate of kerogen to oil increases with thermal maturation, peaking at an Easy% R_o value of 1.0%.
- 3) Over extended storage periods, both bound and free oils in shales of varying maturities remain in an immovable state. The content of immovable oil initially increases with maturity but subsequently decreases.
- 4) *In-situ* conversion of low-to-medium maturity shale in

the upper part of the model can significantly increase movable oil resources in a year, potentially reaching the levels of extractable medium-to-high maturity shale. This study offers foundations for future research and commercial applications in the energy industry by demonstrating the revolutionary potential of *in-situ* conversion technology for unlocking low-to-medium maturity shale oil resources.

Acknowledgements

This research was financially supported by the National Natural Science Foundation of China (Nos. 42472204 and 42272156) and the research on Educational Reform of Hainan Higher Education Institutions (No. Hnjg2024-276).

Supplementary file

<https://doi.org/10.46690/ager.2025.04.08>

Conflict of interest

The authors declare no competing interest.

Open Access This article is distributed under the terms and conditions of the Creative Commons Attribution (CC BY-NC-ND) license, which permits unrestricted use, distribution, and reproduction in any medium, provided the original work is properly cited.

References

- Arrhenius, S. About the reaction rate in the inversion of cane sugar by acids. *Journal of Physical Chemistry*, 1889, 4: 226-248.
- Bai, G., Chen, G., Cai, Z., et al. In situ heating-induced pore structure evolution in low-medium-maturity paleogene lacustrine shale, Bohai Bay Basin, China: Insights from integrated experimental and numerical approaches. *Energy & Fuels*, 2024, 38(15): 14036-14051.
- Behar, F., Lorant, F., Lewan, M. Role of NSO compounds during primary cracking of a Type II kerogen and a Type III lignite. *Organic Geochemistry*, 2008, 39(1): 1-22.
- Braun, R. L., Burnham, A. K. PMOD: A flexible model of oil and gas expulsion, cracking, and expulsion. *Organic Geochemistry*, 1992, 19(1-3): 161-172.
- Burnham, A. K. *Global chemical kinetics of fossil fuels: How to model maturation and pyrolysis*. Cham, Switzerland, Springer, 2017.
- Chen, G., Lu, S., Zhang, J., et al. Estimation of enriched shale oil resource potential in E2s4L of Damintun Sag in Bohai Bay Basin, China. *Energy & Fuels*, 2017, 31(4): 3635-3642.
- Chen, G., Lu, S., Zhang, J., et al. A method for determining oil-bearing pore size distribution in shales: A case study from the Damintun Sag, China. *Journal of Petroleum Science and Engineering*, 2018, 166: 673-678.
- Chen, X., Qu, X., Xu, S., et al. Dissolution pores in shale and their influence on reservoir quality in Damintun Depression, Bohai Bay Basin, East China: Insights from SEM images, N₂ adsorption and fluid-rock interaction experiments. *Marine and Petroleum Geology*, 2020, 117: 104394.
- Dong, Z., Tian, S., Xue, H., et al. A novel method for automatic quantification of different pore types in shale based on SEM-EDS calibration. *Marine and Petroleum Geology*, 2025, 173: 107278.
- Feng, Q., Xu, S., Xing, X., et al. Advances and challenges in shale oil development: A critical review. *Advances in Geo-Energy Research*, 2020, 4(4): 406-418.
- Hou, Y., Yu, R., Li, J., et al. Molecular structure characterization of kerogen in contact metamorphic shales: Insights into the effect of graphitization on organic matter pores. *AAPG Bulletin*. 2024, 108(4): 633-662.
- Hunt, J. M. *Petroleum Geochemistry and Geology*. New York, USA, W. H. Freeman, 1979.
- Hu, T., Pang, X., Jiang, F., et al. Movable oil content evaluation of lacustrine organic-rich shales: Methods and a novel quantitative evaluation model. *Earth-Science Reviews*, 2021, 214: 103545.
- Jarvie, D. M. Shale resource systems for oil and gas: Part 2-shale-oil resource systems. McLean, VA, USA, AAPG Memoir, 2012a.
- Jarvie, D. M. Shale resource systems for oil and gas: Part 1-shale-gas resource systems. McLean, VA, USA, AAPG Memoir, 2012b.
- Jin, J., Jiang, W., Liu, J., et al. Numerical analysis of in situ conversion process of oil shale formation based on thermo-hydro-chemical coupled modelling. *Energies*, 2023, 16(5): 2103.
- Jin, Z. Hydrocarbon accumulation and resources evaluation: Recent advances and current challenges. *Advances in Geo-Energy Research*, 2023, 8(1): 1-4.
- Kang, Z., Zhao, Y., Yang, D. Review of oil shale *in-situ* conversion technology. *Applied Energy*, 2020, 269: 115121.
- Larter, S. R., Huang, H., Snowdon, L., et al. What we do not know about self sourced oil reservoirs: Challenges and potential solutions. Paper SPE 162777 Presented at SPE Canadian Unconventional Resources Conference, Calgary, Alberta, Canada, 30 October-1 November, 2012.
- Lei, Z., Zhang, Y., Yang, Z., et al. Numerical simulation of oil shale in-situ exploration productivity comparison between steam injection and electrical heating. *Applied Thermal Engineering*, 2024, 238: 121928.
- Li, H., Liu, B., Liu, X., et al. Mineralogy and inorganic geochemistry of the Es4 shales of the Damintun Sag, northeast of the Bohai Bay Basin: Implication for depositional environment. *Marine and Petroleum Geology*, 2019b, 110: 886-900.
- Li, J., Lu, S., Chen, G., et al. Correction of light and heavy hydrocarbon loss for residual hydrocarbon S1 and its significance to assessing resource potential of E2s4(2) member in Damintun Sag, Bohai Bay Basin. *Oil & Gas Geology*, 2016, 37(4): 538-545. (in Chinese)
- Li, J., Huang, W., Lu, S., et al. Nuclear magnetic resonance T₁-T₂ map division method for hydrogen-bearing components in continental shale. *Energy & Fuels*, 2018, 32(9): 9043-9054.
- Li, J., Jiang, C., Wang, M., et al. Adsorbed and free hydrocarbons in unconventional shale reservoir: A new insight from NMR T₁-T₂ maps. *Marine and Petroleum Geology*,

- 2020, 116: 104311.
- Li, J., Wang, M., Fei, J., et al. Determination of in situ hydrocarbon contents in shale oil plays. Part 2: Two-dimensional nuclear magnetic resonance (2D NMR) as a potential approach to characterize preserved cores. *Marine and Petroleum Geology*, 2022, 145: 105890.
- Li, M., Chen, Z., Ma, X., et al. Shale oil resource potential and oil mobility characteristics of the Eocene-Oligocene Shahejie Formation, Jiyang Super-Depression, Bohai Bay Basin of China. *International Journal of Coal Geology*, 2019a, 204: 130-143.
- Li, W., Wang, J., Jia, C., et al. Carbon isotope fractionation during methane transport through tight sedimentary rocks: Phenomena, mechanisms, characterization, and implications. *Geoscience Frontiers*, 2024a, 15(6): 101912.
- Li, Y., Chen, G., Cai, Z., et al. Occurrence of methane in organic pores with surrounding free water: A molecular simulation study. *Chemical Engineering Journal*, 2024b, 497, 155597.
- Liao, L., Wang, Y., Chen, C., et al. Kinetic study of marine and lacustrine shale grains using Rock-Eval pyrolysis: Implications to hydrocarbon generation, retention and expulsion. *Marine and Petroleum Geology*, 2018, 89: 164-173.
- Liang, T., Zhan, Z., Zou, Y., et al. Research on type I kerogen molecular simulation and docking between kerogen and saturated hydrocarbon molecule during oil generation. *Chemical Geology*, 2023, 617: 121263.
- Lu, S., Fu, X., Wang, Z., et al. The thermal kinetic models of kerogen to oil and kerogen to gas as well as its calibration. *Scientia Geologica Sinica*, 1996, 31(1): 15-21. (in Chinese)
- Lu, S., Wang, J., Li, W., et al. Economic feasibility and efficiency enhancement approaches for in situ upgrading of low-maturity organic-rich shale from an energy consumption ratio perspective. *Earth Science Frontiers*, 2023, 30(1): 281-295.
- Mehana, M., El-monier, I. Shale characteristics impact on Nuclear Magnetic Resonance (NMR) fluid typing methods and correlations. *Petroleum*, 2016, 2(2): 138-147.
- Pan, Y., Li, M., Sun, Y., et al. Thermo-compression simulation of hydrocarbon generation and expulsion of inter-salt dolomitic shale, Qianjiang Sag, Jiangnan Basin. *Petroleum Geology & Experiment*, 2018, 40(4): 551-558.
- Pepper, A. S., Corvi, P. J. Simple kinetic models of petroleum formation. Part I: Oil and gas generation from kerogen. *Marine and Petroleum Geology*, 1995, 12(3): 291-319.
- Senthil Kumar A. R., Ojha C. S. P., Goyal Manish Kumar, et al. Modeling of suspended sediment concentration at Kasol in India using ANN, Fuzzy logic, and decision tree algorithms. *Journal of Hydrologic Engineering*, 2012, 17(3): 394-404.
- Shi, W., Zheng, H., Wang, B. Numerical simulation of electric heating for oil shale in horizontal wells. *Oil Drilling & Production Technology*, 2014, 36(5): 80-83. (in Chinese)
- Sun, T., Liu, H., Zhang, Y., et al. Numerical simulation and optimization of the *in-situ* heating and cracking process of oil shale. *Oil Shale*, 2023, 40(3): 212.
- Sweeney, J. J., Burnham, A. K. Evaluation of a simple model of vitrinite reflectance based on Chemical kinetics. *AAPG Bulletin*, 1990, 74 (10): 1559-1570.
- Tian, H., He, K., Huangfu, Y., et al. Oil content and mobility in a shale reservoir in Songliao Basin, Northeast China: Insights from combined solvent extraction and NMR methods. *Fuel*, 2024, 357: 129678.
- Tissot, B. P., Welte, D. H. *Petroleum formation and occurrence*, 2nd, rev.enl. ed ed. New York, USA, Springer-Verlag Telos, 1984.
- Wang, G., Yang, D., Kang, Z., et al. Numerical investigation of the in situ oil shale pyrolysis process by superheated steam considering the anisotropy of the thermal, hydraulic, and mechanical characteristics of oil shale. *Energy & Fuels*, 2019, 33(12): 12236-12250.
- Wang, J., Wang, F., Chen, F., et al. Dynamic fractionation of methane carbon isotope during mass transport in coal with bidisperse pore structures: Experiments, numerical modeling, and applications. *Chemical Engineering Journal*, 2024a, 498: 154942.
- Wang, J., Lu, S., Zhang, P., et al. Characterization of shale oil and water micro-occurrence based on a novel method for fluid identification by NMR T2 spectrum. *Fuel*, 2024b, 374: 132426.
- Wu, M. The study of electric heating on hydrocarbon generation and pores evolution of shale in North Songliao Basin (Masteral Dissertation). Qingdao, China University of Petroleum (East China), 2023. (in Chinese)
- Wei, Z., Sheng, J. Changes of pore structures and permeability of the Chang 73 medium-to-low maturity shale during *in-situ* heating treatment. *Energy*, 2022, 248: 123609.
- Xu, L., Wang, Y., Liu, L., et al. Evolution characteristics and model of nanopore structure and adsorption capacity in organic-rich shale during artificial thermal maturation: A pyrolysis study of the Mesoproterozoic Xiamaling marine shale with type II kerogen from Zhangjiakou, Hebei, China. *Energy Exploration & Exploitation*, 2018, 37(1): 493-518.
- Zhang B., Yu C., Cui J., et al. Kinetic simulation of hydrocarbon generation and its application to *in-situ* conversion of shale oil. *Petroleum Exploration and Development*, 2019, 46(6): 1288-1296.
- Zhang, Z., Hou, L., Luo, X., et al. Hydrocarbon generation kinetics and *in-situ* conversion temperature conditions of Chang 7 Member shale in the Ordos Basin, China. *Journal of Natural Gas Geoscience*, 2022, 7(2): 111-119.
- Zhao, W., Hu, S., Hou, L. Connotation and strategic role of *in-situ* conversion processing of shale oil underground in the onshore China. *Petroleum Exploration and Development*, 2018, 45(4): 563-572.